Published in final edited form as:
J Neuropathol Exp Neurol. 2011 July ; 70(7): 596–609. doi:10.1097/NEN.0b013e31822146ca.

p16^{INK4A} and p14^{ARF} Tumor Suppressor Pathways Are Deregulated in Malignant Rhabdoid Tumors

Sriram Venneti, MD, PhD[1], **Paul Le, BS**[2], **Daniel Martinez, BS**[2], **Katherine W. Eaton, BS**[3], **Nikhil Shyam, BS**[4], **Kelly L. Jordan-Sciutto, PhD**[4], **Bruce Pawel, MS**[2], **Jaclyn A. Biegel, PhD**[3,5,6], and **Alexander R. Judkins, MD**[7]

[1]Division of Neuropathology, Department of Pathology and Laboratory Medicine, University of Pennsylvania Medical Center, Philadelphia, Pennsylvania

[2]Divisions of Anatomic Pathology, Department of Pathology and Laboratory Medicine, Philadelphia, Pennsylvania

[3]Division of Human Genetics, Children's Hospital of Philadelphia, Philadelphia, Pennsylvania

[4]Department of Pathology, School of Dental Medicine, University of Pennsylvania School of Medicine, Philadelphia, Pennsylvania

[5]Department of Pathology and Laboratory Medicine, Children's Hospital of Philadelphia, Philadelphia, Pennsylvania

[6]Department of Pediatrics, University of Pennsylvania School of Medicine, Philadelphia, Pennsylvania

[7]Department of Pathology and Laboratory Medicine, Children's Hospital Los Angeles, Keck School of Medicine University of Southern California, Los Angeles, California

Abstract

Malignant rhabdoid tumors (MRT) are aggressive tumors associated with mutations in the *SMARCB1* gene. In experimental systems, the loss of SMARCB1 is hypothesized to alter *p16^{INK4A}* pathways resulting in repression of tumor suppressors. To determine whether these pathways are deregulated in human MRT, we used immunohistochemistry on tissue microarrays to evaluate p16^{INK4A}/E2F1/RB and p14^{ARF}/MDM2/p53 pathways in 25 atypical teratoid/rhabdoid tumors (AT/RT) and 11 non-CNS MRT. p16^{INK4A} was negative or showed focal weak expression. The p16^{INK4A} downstream targets CDK4/cyclin D1/ppRB were variably expressed at moderate to low levels; E2F1 was negative. Unexpectedly, p14^{ARF} expression was seen in many cases, which correlated positively with p53 and inversely with MDM2 immunostaining in AT/RT. *TP53* mutational analysis in 19/25 AT/RT and 8/11 non-CNS MRT cases showed point mutations in only 3 AT/RT cases, suggesting that p53 expression was driven mainly by p14^{ARF}. Finally, nucleophosmin, a protein that stabilizes p53, was positive in the majority of cases and colocalized with p53. Together, these data suggest that in MRT there is deregulation of not only p16^{INK4A}, but also the p14^{ARF} pathway. These results provide insights into cell cycle deregulation in the pathogenesis of human MRT and may aid in the design and evaluation of potential therapies for these tumors.

*Correspondence and reprint requests to: Dr. Alexander R. Judkins, Department of Pathology and Laboratory Medicine, Children's Hospital Los Angeles, Keck School of Medicine, University of Southern California, Los Angeles, CA 19104. Phone: 323-361-4516; Fax: 323-361-4553; ajudkins@chla.usc.edu.

Keywords

Nucleophosmin; $p14^{ARF}$; $p16^{INK4A}$; p53; Rhabdoid tumor

INTRODUCTION

Malignant rhabdoid tumors (MRT) are fatal tumors that occur predominantly in pediatric age groups. When they were first described in 1978, they were thought to be aggressive variants of Wilms tumor but were soon recognized as a distinct entity. Although MRT can occur anywhere in the body, the kidney and the brain are the most common sites of involvement. In the central nervous system (CNS) they are referred to as “atypical teratoid / rhabdoid tumors” (AT/RT) (1).

Insight into the biology of MRT first came from cytogenetic and molecular analysis that showed monosomy of chromosome 22 (2). Further studies demonstrated abnormalities within the *SMARCB1/INI1/SNF5/BAF47* gene in chromosome band 22q11.2 (3). These mutations and/or deletions can be germline or somatic and result in loss of expression of SMARCB1 protein (4–7). This loss can be detected by immunohistochemistry as loss of nuclear protein staining in AT/RT and non-CNS MRT (8). The SMARCB1 protein is a part of the *SWI/SNF* complex, which plays a critical role in chromatin remodeling by influencing histone-DNA interactions in an adenosine triphosphate-dependent manner (9). *Smarcb1* knockout mice are embryonic lethal, but heterozygous *Smarcb1* mice have a normal phenotype at birth and approximately 20% of animals develop sarcoma-like rhabdoid lesions at a median age of 1 year (10). All mice that develop such lesions show acquired deletions in the unaltered second *Smarcb1* allele. Further, conditional bi-allelic *Smarcb1* inactivation results in 100% of mice developing lymphomas and 13% of mice develop sarcoma-like tumors with a rapid median age at onset of 11 weeks, suggesting that bi-allelic inactivation of *Smarcb1* is a requirement for tumor development (11). Interestingly, *SMARCB1* inactivation is also seen in other non-rhabdoid tumors such as epithelioid sarcoma (12), familial schwannomatosis (13), renal medullary carcinoma (14), and in tumors classified by some as extraskeletal myxoid chondrosarcoma (15). This suggests that *SMARCB1* may be a tumor suppressor. Mechanisms by which *SMARCB1* inactivation contributes to either tumor development or progression in these malignancies are poorly understood.

Several studies of cell lines and animal models suggest that loss of SMARCB1 protein results in alterations in key cell cycle regulators. In SMARCB1-deficient cell lines, re-expression of SMARCB1 results in G_1 cell cycle arrest accompanied by both $p16^{INK4A}$ and $p21^{CIP1/WAF1}$ activation (16–19). Inhibition of $p16^{INK4A}$ and $p21^{CIP1/WAF1}$ by inhibitory RNAs reversed cell cycle arrest (18, 19). Furthermore, mice with heterozygous *Smarcb1* deletions show decreased $p16^{INK4a}$ levels (10). While these studies suggest that in cell lines and animal models $p16^{INK4A}$ and $p21^{CIP1/WAF1}$ are downstream of SMARCB1, it is not known if there is decreased expression of $p16^{INK4A}$ and $p21^{CIP1/WAF1}$in human MRT. To address this, we determined expression of both $p21^{CIP1/WAF1}$ and $p16^{INK4A}$ and downstream regulators of $p16^{INK4A}$ - cyclin D1/ CDK4, hyperphosphorylated form of pRb (ppRb) and E2F1 in both AT/RT and non-CNS MRT.

The role of p53 in MRT is also poorly understood. Cell lines established from MRT show overexpression of p53, without associated *TP53* gene mutations (20). On the other hand, missense mutations in *TP53* were reported in 3/6 cases of non-CNS MRT (21). Knockdown of *SMARCB1* in cell lines and animal models results in activation of p53 (22, 23). Intriguingly, combined inactivation of Smarcb1 and p53, but not Rb or $p16^{ink4a}$, leads to accelerated development of MRT in mouse models (23, 24). These data have led to the

hypothesis that 2 successive hits involving *SMARCB1* and *TP53* may contribute to malignant transformation and tumor development. To evaluate the role of p53 in MRT, we studied the expression of p53 and determined *TP53* mutational status in AT/RT and non-CNS MRT. We also studied the relationship of p53 expression with its regulators $p14^{ARF}$/MDM2 in AT/RT and non-CNS MRT.

MATERIALS AND METHODS

Cases

A tissue microarray (TMA) comprised of 36 AT/RT and 16 non-CNS MRT cases collected between 1985 and 2008 from the Department of Pathology Children's Hospital of Philadelphia was constructed following previously established methods (25). Briefly, representative tumor areas were delineated on hematoxylin and eosin sections and matched directly to corresponding blocks. A cylindrical portion (0.6 mm) of tumor tissue was transferred into the recipient block at specific positions to form a TMA. Normal CNS tissue and non-CNS tissues were included in the block. Evaluation of the TMA confirmed that the appearance of tumor tissue cores corresponded to the original blocks. Loss of expression of SMARCB1 was confirmed in all cases by immunohistochemical staining of both the original donor blocks and the TMAs. Cores with artifacts, low cellularity, cautery effect or viable tumor less than 90% per core were not analyzed. To assess the relationship between the different variables, only cores that showed preserved tumor for all the different markers were considered. Out of 36 cases of AT/RT and 16 cases of non-CNS MRT in the TMAs, 25 AT/RT cases and 11 non-CNS MRT cases met these criteria. These patients ranged in age from 6 to 240 months with a median age of 28 months; 22 were males and 14 were females (Table 1).

Immunohistochemistry

Tissue microarrays were stained with the primary antibodies listed in Table 2. Sections were soaked in xylene (EMD Chemicals Gibbstown, NJ) for 30 minutes, rinsed in 2 changes of xylene for 5 minutes each, and then rehydrated in a series of descending concentrations of ethanol (Fisher Scientific Fair Lawn, NJ). Slides were treated with 0.3% H_2O_2/methanol (AppliChem Darmstadt, Germany/Fisher Scientific) for 30 minutes to block endogenous peroxide. Heat-induced epitope retrieval was achieved by treating slides in a pressure cooker with 0.01M Citrate buffer (Vector Laboratories, Burlingame, CA), pH 7.6. Slides were then rinsed in 0.1M Tris Buffer with Tween 20 (both from Dako), then blocked with 2% fetal bovine serum (Sigma-Aldrich St. Louis, MO) for 5 minutes. Slides were subsequently incubated with the primary antibody at specified concentrations for 1 hour at room temperature (RT) or overnight at 4°C (Table 2). Slides were rinsed in Tris and then incubated with biotinylated anti-mouse IgG or anti-goat IgG (Vector) for 30 minutes at RT. After rinsing in Tris, slides were incubated with the avidin biotin complex (Vector) for 30 minutes at RT, followed by incubation with 3, 3' diaminobenzidine (Dako) for 10 minutes at RT. Slides were then rinsed, dehydrated through a series of ascending concentrations of ethanol and xylene, and coverslipped. Optimal staining conditions for any given antibody were determined using appropriate positive and negative controls.

Scoring of Tissue Microarrays

Each slide was scanned using the Aperio Scanscope Scanner (Aperio, Vista, CA), and viewed through Aperio's ImageScope software program. Staining for each antibody was considered positive when reaction products were localized in the expected cellular component. Staining intensity was determined using a semiquantitative system of negative (0), weak (1+), moderate (2+) and strong (3+), as illustrated in Figure 1. The percentage of positive tumor cells in each core was roughly estimated and multiplied by the staining

intensity to provide a semiquantitative measure for each antibody for each core. To determine if there was an association of longer sample storage duration and lower staining intensities, the staining intensities for each individual marker were correlated against time (numbers of years in storage); no significant relationships were observed for any of the markers. Further, staining intensities for all markers were cumulatively correlated with the number of years in storage to assess any global trends and no significant relationships were observed (spearman r = 0.0169, p = 0.8250).

PCR and DNA Sequencing Analyses

PCR and DNA sequence analyses were performed on 19/25 AT/RT and 8/11 non-CNS MRT cases due to limited tissue availability using primers for exons 2–9 of *TP53*, as previously described (26, 27). PCR products were sequenced utilizing the BigDye Terminator v3.1 Cycle Sequencing Kit (Applied Biosystems, Foster City, CA), per the manufacturer's protocol. Sequencing products were analyzed on a 3730 DNA Analyzer (Applied Biosystems) by the Children's Hospital of Philadelphia Nucleic Acid/Protein Core (27).

Immunofluorescence Double Labeling

For immunofluorescence double labeling antibodies to nucleophosmin (NPM) (1:100) or phosphorylated nucleophosmin (pNPM) (1:50) were each used in conjunction with p53 (1:25) to stain formalin fixed-paraffin embedded slides. Slides were rinsed in 2 changes of xylene for 5 minutes each then rehydrated in a series of descending concentrations of ethanol. Sides were treated in a pressure cooker with 0.01M Citrate buffer pH 7.6. After cooling, slides were rinsed in 0.1M Tris Buffer then blocked with 2% fetal bovine serum for 15 minutes. Slides were then incubated with the primary antibody pairs overnight at 4°C. Slides were again rinsed then incubated with Alexa 594 anti-Rabbit and Alexa 488 Anti-Mouse (both from Invitrogen, Carlsbad, CA) at a 1:200 dilution for 1 hour at RT. Slides were rinsed then counterstained for 5 minutes in DAPI Hydrochloride (Sigma-Aldrich). Slides were rinsed, then coverslipped with Mowiol 4–88 (Sigma-Aldrich).

Statistical Analysis

Data were analyzed using PRISM software (Graphpad, San Diego, CA). ANOVA with 95% confidence intervals were used to determine differences between $p16^{INK4A}$, $p21^{CIP1/WAF1}$ and $p14^{ARF}$ staining. Non-parametric correlations using 95% confidence intervals were performed to quantify the relationship between various immunohistochemical markers. Results from correlation analyses are represented by r^2, the Spearman's coefficient.

RESULTS

AT/RT and Non-CNS MRT Show Negative or Focal Weak $p21^{CIP1/WAF1}$ and $p16^{INK4A}$ Expression with Comparatively Higher $p14^{ARF}$ Protein Expression

Most cases of AT/RT (22/25, 88%) and 6/11 (55%) non-CNS MRT cases were negative for $p21^{CIP1/WAF1}$. Focal weak (1+) immunostaining with $p21^{CIP1/WAF1}$ was noted in 3/25 (12%) AT/RT cores and 5/11 (45%) non-CNS MRT cores (Fig. 2; Table 3). Similarly, no staining for $p16^{INK4A}$ was present in 17/25 AT/RT (68%) and 4/11 (36%) non-CNS MRT cases. The remaining cases showed focal weak (1+) immunostaining with $p16^{INK4A}$ in 8/25 (32%) AT/RT cores and 6/11 (55%) non-CNS MRT cores. A single non-CNS MRT core showed strong (3+) staining with $p16^{INK4A}$ (Fig. 2; Table 3).

In contrast, 21/25 (84%) and 11/11 (100%) non-CNS MRT showed staining with $p14^{ARF}$. Weak $p14^{ARF}$ (1+) staining in 6/25 (24%), moderate (2+) staining in 13/25 (52%) and strong (3+) staining in 2/25 (8%) were observed in AT/RT cases. No $p14^{ARF}$ staining was

seen in 4/25 (16%) of AT/RT cases. All Non-CNS MRT cases were positive for $p14^{ARF}$ ranging from weak (1+) staining in 3/11 (27%), moderate (2+) staining in 6/11 (55%) to strong (3+) staining in 2/11 (18%) cases (Fig. 2; Table 3).

Expression Profiles of $p16^{INK4A}$ Downstream Targets CDK4, Cyclin D1, ppRB, and E2F1

Because $p16^{INK4A}$ was either absent or focally weakly expressed, we examined the expression pattern of $p16^{INK4A}$ downstream targets: CDK4, cyclin D1, ppRB, and E2F1 (Fig. 1). CDK4 expression was noted in 13/25 (52%) of AT/RT (1+ staining in 12/25 (48%) and 2+ staining in 1/25 (4%) cores) and 8/11 (73%) of non-CNS MRT (1+ staining in 7/11 (64%) and 2+ staining in 1/11 (9%) cores). 12/25 (48%) cases of AT/RT and 3/11 (27%) non-CNS MRT were negative for CDK4 (Fig. 3; Table 3).

20/25 (80%) AT/RT cases and 6/11 (55%) of non-CNS MRT were negative for cyclin D1 expression. Weak (1+) cyclin D1 expression was noted in 5/25 (20%) of AT/RT and 6/11 (45%) of non-CNS MRT (Fig. 3; Table 3).

ppRB was positive in 16/25 (64%) cases of AT/RT (1+ staining in 14/25 (56%) and 2+ staining in 2/25 (8%) cores). In non-CNS MRT cases, 10/11 (91%) were positive for ppRB (weak staining in 6/11 (56%), moderate staining in 3/11 (27%) and strong staining in 1/11 (9%) of cores). No staining was observed in 9/25 (36%) of AT/RT cases and 1/11 (9%) of non-CNS MRT cases for ppRB (Fig. 4; Table 3). Surprisingly, no E2F1 was identified in any of the cases (Fig. 4; Table 3). The absence of E2F1 expression was confirmed in 2 independent laboratories (A.R.J. and K.J.S.) using appropriate positive (i.e. several carcinomas and normal tissue samples) and negative controls (data not shown). Additionally, no significant correlations were observed between $p16^{INK4A}$, CDK4, cyclin D1, ppRB, and E2F1 (data not shown).

AT/RT and Non-CNS MRT Show p53 Protein Expression that Correlates with $p14^{ARF}$

Positive immunostaining with p53 was noted in 84% (21/25) AT/RT, and 100% (11/11) non-CNS MRT cores. Weak staining was seen in 16/25 (64%) of AT/RT cases. Similarly, weak staining was seen in 5/11 (45%) non-CNS MRT cases. Moderate staining was seen in 5/25 (20%) AT/RT cases and 4/11 (36%) non-CNS MRT cases. Strong diffuse immunoreactivity was seen in 2/11 (14%) non-CNS MRT cases (Fig. 5; Table 3). No staining was observed in 4/25 (16%) of AT/RT cases.

Positive correlations were observed with p53 and $p14^{ARF}$ protein expression in both AT/RT ($r^2 = 0.6159$, $p = 0.001$) and non-CNS MRT cases ($r^2 = 0.7446$, $p = 0.0086$) (Fig. 6). No significant correlations were observed between p53 with $p16^{INK4A}$ or $p21^{CIP1/WAF1}$ in both AT/RT and non-CNS MRT.

MDM2, a downstream regulator of $p14^{ARF}$ was positive in 18/25 (72%) of AT/RT cases (weak staining in 14/25 (56%) and moderate staining in 4/25 (16%). In non-CNS MRT cases 9/11 (82%) showed weak staining. No staining was detected in 7/25 (28%) cases of AT/RT and 2/11 (18%) of non-CNS MRT cases for MDM2 (Fig. 5; Table 3). Negative correlation was observed between p53 and MDM2 in AT/RT ($r^2 = -0.4938$, $p = 0.0229$), but not in non-CNS MRT ($r^2 = -0.1431$ $p = 0.6747$) (Fig. 6).

TP53 Mutational Analysis

Due to limitations in tissue availability, *TP53* mutational analyses were conducted on 19 AT/RT and 8 non-CNS MRT cases. Polymorphisms in *TP53* were seen in all cases analyzed; the most common of these was a proline to arginine change in codon 72 (c. 215C>G). Any changes found that were not listed in the International Agency for Research

on Cancer database of known *TP53* polymorphisms were classified as mutations (www-p53.iarc.fr). Four *TP53* mutations (2 missense and 2 silent) were observed in 3/19 (16%) of the AT/RT cases (Table 1). These included c.722C>T (Ser>Phe), c.246G>A (Pro>Pro), c.467G>A (Arg>His) and c.582T>C (Leu>Leu) (Table 1). No mutations were observed in the non-CNS MRT cases (Table 1).

AT/RT and Non-CNS MRT Show NPM and pNPM Expression

NPM is a nuclear phosphoprotein that may associate with $p14^{ARF}$ and p53 to stabilize these factors (28, 29). Because both $p14^{ARF}$ and p53 were expressed in AT/RT and non-CNS MRT, we examined NPM and pNPM expression. We found that all 25 AT/RT and 11 non-CNS MRT were positive for NPM (100%). In AT/RT cases, 17/25 (68%) cases showed weak staining, 6/25 (24%) showed moderate staining and 2/25 (8%) showed strong staining (Fig. 7; Table 3). Similarly, in the non-CNS MRT cases 10/11 (91%) showed weak (1+) staining and 1/11 (9%) showed strong (3+) staining with NPM. Weak staining was seen in 22/25 (88%) and moderate staining was seen in 2/25 (8%) of AT/RT cases with pNPM. 3/25 (12%) AT/RT cases were negative for pNPM. All 11/11 (100%) non-CNS MRT cases showed weak staining with pNPM (Fig. 7; Table 3). Finally, immunofluorescent double labeling showed that both NPM and pNPM colocalized in nuclei with p53 (Fig. 8).

DISCUSSION

MRT are lethal cancers that predominantly arise in pediatric age groups in the CNS, kidney, and soft tissues (30, 31). Mutations and deletions in the *SMARCB1* gene with a corresponding loss of protein expression are associated with AT/RT and non-CNS MRT (3, 5, 6). SMARCB1 is a part of the SWI/SNF complex and insights from animal models and cell culture systems support the role of SMARCB1 as a tumor suppressor (10, 22, 32).

The mechanisms by which loss of the SMARCB1 protein contributes to tumorigenesis are poorly understood. Current hypotheses implicate alterations in cell cycle regulators, but it is not known whether these pathways are altered in human MRT.

The $p16^{INK4A}$ Pathway in MRT

$p16^{INK4A}$ is a key cell cycle regulator implicated in many cancers. Increased levels of $p16^{INK4A}$ result in inhibition of the CDK4/Cyclin D1 complex, retaining RB in its anti-proliferative hypophosphorylated state, which sequesters E2F1, preventing activation of genes needed for cell cycle entry (Fig. 1C) (33). Data from cell lines and animal models suggest that $p16^{INK4A}$ is a direct downstream target of SMARCB1 (16–18, 23). Restored SMARCB1 in rhabdoid cell lines binds to the $p16^{INK4A}$ promoter and enhances its expression leading to cellular senescence (17, 18). Conversely, mice generated with heterozygous *Smarcb1* deletions show decreased $p16^{INK4A}$ levels (10). Cell lines generated from MRT contain virtually undetectable levels of $p16^{INK4A}$ (16, 34). Further, low levels of $p16^{INK4A}$ were detected in *SMARCB1* deleted cell lines with after long exposures on western blot analyses suggesting that this was due to reduced transcription of *$p16^{INK4}$* but not gene deletion (16). Consistent with this observation, we did not detect any *$p16^{INK4A}$* deletions using high resolution single nucleotide polymorphism-based oligonucleotide array analysis (6). These data predict that a loss of SMARCB1 would result in absent or decreased $p16^{INK4A}$ levels in human MRT. In accordance with this prediction, our studies show that $p16^{INK4A}$ is absent or weakly focally expressed in both AT/RT and non-CNS MRT (Fig. 2).

Because $p16^{INK4A}$ is decreased or lost in experimental systems, much emphasis has been placed on the $p16^{INK4A}$ downstream targets (i.e. cyclin D1/ CDK4-RB-E2F1) as central to the pathogenesis of MRT (Fig. 1C). Data on these downstream targets of $p16^{INK4A}$ in

experimental systems of MRT appear contradictory or difficult to interpret. SMARCB1-deficient cell lines that showed absent or low expression of p16INK4A exhibited no amplification of cyclin D1 (16). Similarly, re-expression of SMARCB1 did not alter CDK4 or cyclin D1 expression in cell lines (35). In contrast, others report decreased transcription of cyclin D1 with re-expression of SMARCB1 in an HDAC-dependent manner (36). Pharmacological inhibition of cyclin D1 induced cell cycle arrest and apoptosis both in rhabdoid cell lines and in a xenograft model of MRT (37). Despite these differences in cell culture systems, in vivo data from mice with heterozygous Smarcb1 deletions show decreased tumor development on ablation of cyclin D1 (38). We noted focal expression of cyclin D1 in 20% of AT/RT and 45% of MRT similar to focal cyclin D1 expression reported by others in a small number of AT/RT cases (36, 39). CDK4, the kinase partner of cyclin D1, showed similar low focal expression in 52% of AT/RT and 45% of non-CNS MRT (Fig. 3).

Re-expression of SMARCB1 activated RB resulting in G1 cell cycle arrest (16). However, this study showed that SMARCB1-deficient cell lines that contain absent or low expression of $p16^{INK4A}$ show normal RB protein levels, suggesting that loss of SMARCB1 does not upregulate RB, despite low levels of $p16^{INK4A}$ (16). Regulation of cyclin D1 with re-expression of SMARCB1 was dependent on HDAC but was independent of RB function (36). Furthermore, co-inactivation of SMARCB1 and RB had no significant effect on the rate of tumor formation in an animal model of MRT (23). Mice with compound heterozygous inactivation for *Rb* and *Smarcb1* developed pituitary tumors with no differences in the rate of tumor development on inactivation of either protein alone (40). These studies suggest that *RB* may not be critical to *SMARCB1* deletion induced oncogenesis attributed to redundant tumor-suppressing capabilities of these 2 proteins (23). Consistent with this hypothesis, we noted weak to moderate expression of hyperphosphorylated RB in both AT/RT and MRT cases, similar to a previous report (41) (Fig. 4).

E2F1 is downstream of RB and is released upon hyperphosphorylation of RB. Re-expression of SMARCB1 in MRT cell lines showed markedly lower levels of E2F1 and some target genes of E2F such as CDC6 and cyclin A, but not others such as cyclin E, CDK2 or B-myb (35). Gene profiling experiments report decreased E2F-related genes in rhabdoid cells lines with SMARCB1 re-expression (42). Similarly, gene profiling of murine embryonic fibroblasts with deleted *Smarcb1* show increased E2F target genes (23). In contrast to these data, *Smarcb1* deletion in murine embryonic fibroblasts caused no alterations in *E2f1* levels or E2F target genes (43). In our study, despite modest expression of hyperphosphorylated RB, all AT/RT and non-CNS MRT cases were strikingly negative for E2F1 (Fig. 4), similar to data reported by Yaniv et al (43).

These discrepancies in downstream regulators of $p16^{INK4A}$ may be due to differences in various MRT model systems, but may also reflect the complexity of pathways that regulate the cell cycle. It is tempting to speculate that lowered $p16^{INK4A}$ may drive oncogenic pathways distinct from those regulated by E2F1. However, we recognize the limitations of our study, including those applicable to the examination of human tissues, such as variability in fixation times, processing methods and procurement. Furthermore, the complex dynamic and temporal interactions intrinsic to cell cycle proteins make clinically derived human tumor samples a less than optimal system for resolving these questions. Nevertheless, the ability to interrogate these pathways in human tumors is a valuable addition to previously published data derived from various model systems. Similar discrepancies have been noted with expression of tyrosine kinase receptors (e.g. platelet-derived growth factor receptor and epidermal growth factor receptor) on comparing experimental systems with human MRT samples (44, 45).

p14^{ARF} and p53 in MRT

The role of p53 and p14^{ARF} in MRT is less studied and poorly understood. p14^{ARF} binds to MDM2 to prevent p53 degradation (Fig. 1). Once stabilized, p53 may regulate several functions including cell cycle arrest and apoptosis (46). Altered expression of p53 has been noted in medulloblastoma, another CNS embryonal tumor, and was initially reported to be associated with p53 mutations and a worse prognosis (47). However, subsequent studies have not confirmed this (48). In mouse models of MRT, *Smarcb1* loss leads to marked upregulation of p53 (23). The best evidence that *p53* is important in MRT pathogenesis is from studies of animal models in which homozygous or heterozygous *p53* inactivation cooperates with inactivation of *Smarcb1* to accelerate latency of tumor formation (23, 24). More importantly, no synergy was observed between inactivation of *Smarcb1* and either p16^{INK4a} or *Rb*, suggesting a specific role for *p53* in the pathogenesis of MRT (23).

There are 2 main hypotheses regarding the function of *p53* in MRT. The first is the double hit hypothesis, which postulates that mutations in both *SMARCB1* and *p53* contribute to tumorigenesis. Data supporting this hypothesis are limited. Increased p53 expression by immunohistochemistry was described in 5/6 non-CNS MRT, 3 of which showed *p53* missense mutations (21). In a study involving CNS embryonal tumors, 2/3 AT/RT cases showed staining for p53 (49). No definitive correlation exists between p53 expression by immunohistochemistry and *TP53* mutations in either CNS or non-CNS malignancies (50–54). There has been no systematic study of p53 immunohistochemistry and its relation to the mutational status in MRT. In our cohort, 84% of AT/RT cases and 100% of non-CNS MRT cases showed p53 positivity. Despite this staining profile, only 3/19 AT/RT and none of the non-CNS MRT cases showed *TP53* mutations (Table 1). Of the 3 cases, only case #18 showed both strong p53 immunoreactivity and a *TP53* mutation. No 17p deletions or loss of heterozygosity were observed by high resolution single nucleotide polymorphism array analysis (6). Interestingly, *TP53* polymorphisms were observed in all the analyzed AT/RT and non-CNS MRT cases. The significance of this finding is not known. Overall, these data do not support the *TP53* / *Smarcb1* 2 gene hit hypothesis.

Alternatively, it has been hypothesized that intact SMARCB1 and p53 may cooperate in preventing oncogenesis in an unknown manner (23). Upregulation of p53 in a *SMARCB1*-deficient state may be a mechanism used to combat prooncogenic effects of *SMARCB1* loss that are eventually overcome when MRT develop (23, 43). Unexpectedly, we found that p53 expression correlated positively with p14^{ARF} expression in MRT. Negative correlations were observed with MDM2 in AT/RT cases. These data together raise the possibility that p53 expression in MRT may be driven by p14^{ARF}. We sought to determine if expression of p53 or p14^{ARF} had any prognostic implications. Unfortunately, survival data was available only on 14/25 AT/RT cases and 6/11 non-CNS MRT cases. Cases that expressed p53/p14^{ARF} showed a non-significant trend towards greater survival periods than cases that did not show expression (data not shown). This may be due to the relatively small number of samples with available survival data. Another possibility is that the uniform dismal prognosis of MRT (average survival time of 12 months after presentation) may not allow for clear prognostic indicators.

As with the p16^{INK4A} pathway, experimental data regarding p53 and p14^{ARF} in MRT models also vary. Cell culture and animal models of MRT do not show changes in p14^{ARF} expression with *SMARCB1* loss (18, 23). Human carcinoma cells with *SMARCB1* knockdown show decreased p53 expression (55), but (similar to our data) Yaniv et al observed increased levels of p53 and p14^{ARF} in murine embryonic fibroblasts with *Smarcb1* deletion (43).

One of the functions of $p21^{WAF1/CIP1}$ is to mediate the tumor suppressor activity of p53 by inducing growth arrest, differentiation or senescence (56). In the context of MRT, $p21^{WAF1/CIP1}$ is activated in p53-dependent and -independent fashions at the onset of SMARCB1 induced growth arrest (19). Interestingly, the expression of $p21^{CIP1/WAF1}$ upregulation precedes $p16^{INK4A}$, suggesting a complex temporal regulation by SMARCB1 (19). Our results show negative or focal weak expression of $p21^{CIP1/WAF1}$ in parallel with these data (Fig. 2). Furthermore, no correlations were observed between p53 and $p21^{CIP1/WAF1}$, suggesting that downregulation of *p21*$^{CIP1/WAF1}$ may also occur independently of p53 expression (19).

NPM in MRT

NPM is a nuclear phosphoprotein that can regulate cellular proliferation and growth suppression and is frequently expressed in many human tumors such as gastric (57), ovarian (58) and colon (59) carcinomas. Genetic alterations result in *NPM* fusion with 1) retinoic acid receptor-a (*RARA*) seen in acute promyelocytic leukemia (APL); 2) anaplastic lymphoma kinase (*ALK*) in anaplastic large cell lymphoma (ALCL); and 3) myelodysplasia/ myeloid leukemia factor 1 (*MLF1*) in myelodysplastic syndromes (60, 61). Amongst its many functions, NPM associates with $p14^{ARF}$ in the nucleolus and stabilizes it by retarding its turnover (28). NPM can also interact with MDM2 and protect p53 from MDM2-mediated degradation (62). Finally, NPM can interact with p53 itself and stabilize p53 (29). Because our results suggest activation of p53 downstream of $p14^{ARF}$, we evaluated NPM expression in MRT and found that all of the MRT cases showed nuclear staining for NPM. Phosphorylation of NPM is important for mitotic function of cells (63) and we found that 88% of AT/RT cases and 100% of non-CNS MRT cases were immunopositive for pNPM. Further, both NPM and pNPM colocalized with p53 in MRT. Thus, NPM may play a role in stabilizing p53, as well as function in regulating mitotic activity in MRT. Mechanisms that mediate NPM activation in MRT are not currently known.

Based on cell culture systems and animal models, the deregulation of cell cycle proteins (e.g. those downstream of $p16^{INK4A}$) is a leading hypothesis relating *SMARCB1* loss with oncogenesis in MRT and it is imperative to determine whether the same pathways apply to human MRT for the development of therapies. TMAs enabled assessing multiple AT/RT and non-CNS MRT cases simultaneously but a drawback of this approach is sampling bias, especially in the context of the heterogeneity of MRT. Another limitation lies in the semiquantitative approach in comparing expression of various proteins. Antibodies have different avidities to their respective antigens and comparison of expression of various proteins under different staining conditions (e.g. concentrations and incubation times) may be challenging.

Our data show both similarities and differences in comparison to experimental systems. We observe low or no expression of $p16^{INK4A}$ and $p21^{CIP1/WAF1}$. No E2F1 expression was noted despite focal expression of cyclin D1, CDK4 and ppRB. In contrast, we observed the expression of p53 in the absence of *TP53* mutations, which was correlated with changes in the $p14^{ARF}$ / MDM2 pathway. Our data support the hypothesis that *SMARCB1* and *TP53* may cooperate in preventing oncogenesis. Upregulation of p53 in MRT may be an anti-oncogenic mechanism that is overcome by the effects of *Smarcb1* inactivation. The expression of markers associated with $p14^{ARF}$ / MDM2 / p53 in human MRT suggest that this pathway may explain the oncogenic effects of loss of SMARCB1 expression, and provide a potential target for designing therapies to treat MRT.

Acknowledgments

This work was supported in part by a grant from the NIH (R0146274) to J.A.B.

REFERENCES

1. Rorke LB, Packer RJ, Biegel JA. Central nervous system atypical teratoid/rhabdoid tumors of infancy and childhood: definition of an entity. J Neurosurg. 1996; 85:56–65. [PubMed: 8683283]
2. Biegel JA, Rorke LB, Emanuel BS. Monosomy 22 in rhabdoid or atypical teratoid tumors of the brain. N Engl J Med. 1989; 321:906. [PubMed: 2770830]
3. Versteege I, Sevenet N, Lange J, et al. Truncating mutations of hSNF5/INI1 in aggressive paediatric cancer. Nature. 1998; 394:203–6. [PubMed: 9671307]
4. Biegel JA, Allen CS, Kawasaki K, et al. Narrowing the critical region for a rhabdoid tumor locus in 22q11. Genes Chromosomes Cancer. 1996; 16:94–105. [PubMed: 8818656]
5. Biegel JA, Zhou JY, Rorke LB, et al. Germ-line and acquired mutations of INI1 in atypical teratoid and rhabdoid tumors. Cancer Res. 1999; 59:74–9. [PubMed: 9892189]
6. Jackson EM, Sievert AJ, Gai X, et al. Genomic analysis using high-density single nucleotide polymorphism-based oligonucleotide arrays and multiplex ligation-dependent probe amplification provides a comprehensive analysis of INI1/SMARCB1 in malignant rhabdoid tumors. Clin Cancer Res. 2009; 15:1923–30. [PubMed: 19276269]
7. Bruggers CS, Bleyl SB, Pysher T, et al. Clinicopathologic comparison of familial versus sporadic atypical teratoid/rhabdoid tumors (AT/RT) of the central nervous system. Pediatr Blood Cancer. Jul 1.2011 56:1026–31. [PubMed: 20848638]
8. Judkins AR, Mauger J, Ht A, Rorke LB, et al. Immunohistochemical analysis of hSNF5/INI1 in pediatric CNS neoplasms. Am J Surg Pathol. 2004; 28:644–50. [PubMed: 15105654]
9. Reisman D, Glaros S, Thompson EA. The SWI/SNF complex and cancer. Oncogene. 2009; 28:1653–68. [PubMed: 19234488]
10. Roberts CW, Galusha SA, McMenamin ME, et al. Haploinsufficiency of Snf5 (integrase interactor 1) predisposes to malignant rhabdoid tumors in mice. Proc Natl Acad Sci U S A. 2000; 97:13796–800. [PubMed: 11095756]
11. Roberts CW, Leroux MM, Fleming MD, et al. Highly penetrant, rapid tumorigenesis through conditional inversion of the tumor suppressor gene Snf5. Cancer Cell. 2002; 2:415–25. [PubMed: 12450796]
12. Hornick JL, Dal Cin P, Fletcher CD. Loss of INI1 expression is characteristic of both conventional and proximal-type epithelioid sarcoma. Am J Surg Pathol. 2009; 33:542–50. [PubMed: 19033866]
13. Hulsebos TJ, Plomp AS, Wolterman RA, et al. Germline mutation of INI1/SMARCB1 in familial schwannomatosis. Am J Hum Genet. 2007; 80:805–10. [PubMed: 17357086]
14. Cheng JX, Tretiakova M, Gong C, et al. Renal medullary carcinoma: rhabdoid features and the absence of INI1 expression as markers of aggressive behavior. Mod Pathol. 2008; 21:647–52. [PubMed: 18327209]
15. Kohashi K, Oda Y, Yamamoto H, et al. SMARCB1/INI1 protein expression in round cell soft tissue sarcomas associated with chromosomal translocations involving EWS: a special reference to SMARCB1/INI1 negative variant extraskeletal myxoid chondrosarcoma. Am J Surg Pathol. 2008; 32:1168–74. [PubMed: 18580682]
16. Betz BL, Strobeck MW, Reisman DN, et al. Re-expression of hSNF5/INI1/BAF47 in pediatric tumor cells leads to G1 arrest associated with induction of p16ink4a and activation of RB. Oncogene. 2002; 21:5193–203. [PubMed: 12149641]
17. Chai J, Charboneau AL, Betz BL, et al. Loss of the hSNF5 gene concomitantly inactivates p21CIP/WAF1 and p16INK4a activity associated with replicative senescence in A204 rhabdoid tumor cells. Cancer Res. 2005; 65:10192–8. [PubMed: 16288006]
18. Oruetxebarria I, Venturini F, Kekarainen T, et al. P16INK4a is required for hSNF5 chromatin remodeler-induced cellular senescence in malignant rhabdoid tumor cells. J Biol Chem. 2004; 279:3807–16. [PubMed: 14604992]
19. Kuwahara Y, Charboneau A, Knudsen ES, et al. Reexpression of hSNF5 in malignant rhabdoid tumor cell lines causes cell cycle arrest through a p21(CIP1/WAF1)-dependent mechanism. Cancer Res. 2010; 70:1854–65. [PubMed: 20179200]

20. Rosson GB, Hazen-Martin DJ, Biegel JA, et al. Establishment and molecular characterization of five cell lines derived from renal and extrarenal malignant rhabdoid tumors. Mod Pathol. 1998; 11:1228–37. [PubMed: 9872656]
21. Kinoshita Y, Shiratsuchi H, Tamiya S, et al. Mutations of the p53 gene in malignant rhabdoid tumors of soft tissue and the kidney: immunohistochemical and DNA direct sequencing analysis. J Cancer Res Clin Oncol. 2001; 127:351–8. [PubMed: 11414195]
22. Kato H, Honma R, Sanda T, et al. Knock down of hSNF5/Ini1 causes cell cycle arrest and apoptosis in a p53-dependent manner. Biochem Biophys Res Commun. 2007; 361:580–5. [PubMed: 17669367]
23. Isakoff MS, Sansam CG, Tamayo P, et al. Inactivation of the Snf5 tumor suppressor stimulates cell cycle progression and cooperates with p53 loss in oncogenic transformation. Proc Natl Acad Sci U S A. 2005; 102:17745–50. [PubMed: 16301525]
24. Delbove J, Kuwahara Y, Mora-Blanco EL, et al. Inactivation of SNF5 cooperates with p53 loss to accelerate tumor formation in Snf5(+/−);p53(+/−) mice. Mol Carcinog. 2009; 48:1139–48. [PubMed: 19676100]
25. Winter C, Pawel B, Seiser E, et al. Neural cell adhesion molecule (NCAM) isoform expression is associated with neuroblastoma differentiation status. Pediatr Blood Cancer. 2008; 51:10–6. [PubMed: 18213713]
26. Nichols KE, Heath JA, Friedman D, et al. TP53, BRCA1, and BRCA2 tumor suppressor genes are not commonly mutated in survivors of Hodgkin's disease with second primary neoplasms. J Clin Oncol. 2003; 21:4505–9. [PubMed: 14673037]
27. Dougherty MJ, Santi M, Brose MS, et al. Activating mutations in BRAF characterize a spectrum of pediatric low-grade gliomas. Neuro Oncol. 2010
28. Bertwistle D, Sugimoto M, Sherr CJ. Physical and functional interactions of the Arf tumor suppressor protein with nucleophosmin/B23. Mol Cell Biol. 2004; 24:985–96. [PubMed: 14729947]
29. Colombo E, Marine JC, Danovi D, et al. Nucleophosmin regulates the stability and transcriptional activity of p53. Nat Cell Biol. 2002; 4:529–33. [PubMed: 12080348]
30. Rorke LB, Packer R, Biegel J. Central nervous system atypical teratoid/rhabdoid tumors of infancy and childhood. J Neurooncol. 1995; 24:21–8. [PubMed: 8523069]
31. Roberts CW, Biegel JA. The role of SMARCB1/INI1 in development of rhabdoid tumor. Cancer Biol Ther. 2009; 8:412–6. [PubMed: 19305156]
32. Klochendler-Yeivin A, Fiette L, Barra J, et al. The murine SNF5/INI1 chromatin remodeling factor is essential for embryonic development and tumor suppression. EMBO Rep. 2000; 1:500–6. [PubMed: 11263494]
33. Kim WY, Sharpless NE. The regulation of INK4/ARF in cancer and aging. Cell. 2006; 127:265–75. [PubMed: 17055429]
34. Kuroda H, Moritake H, Sawada K, et al. Establishment of a cell line from a malignant rhabdoid tumor of the liver lacking the function of two tumor suppressor genes, hSNF5/INI1 and p16. Cancer Genet Cytogenet. 2005; 158:172–9. [PubMed: 15796965]
35. Versteege I, Medjkane S, Rouillard D, et al. A key role of the hSNF5/INI1 tumour suppressor in the control of the G1-S transition of the cell cycle. Oncogene. 2002; 21:6403–12. [PubMed: 12226744]
36. Zhang ZK, Davies KP, Allen J, et al. Cell cycle arrest and repression of cyclin D1 transcription by INI1/hSNF5. Mol Cell Biol. 2002; 22:5975–88. [PubMed: 12138206]
37. Alarcon-Vargas D, Zhang Z, Agarwal B, et al. Targeting cyclin D1, a downstream effector of INI1/hSNF5, in rhabdoid tumors. Oncogene. 2006; 25:722–34. [PubMed: 16302003]
38. Tsikitis M, Zhang Z, Edelman W, et al. Genetic ablation of Cyclin D1 abrogates genesis of rhabdoid tumors resulting from Ini1 loss. Proc Natl Acad Sci U S A. 2005; 102:12129–34. [PubMed: 16099835]
39. Fujisawa H, Misaki K, Takabatake Y, et al. Cyclin D1 is overexpressed in atypical teratoid/rhabdoid tumor with hSNF5/INI1 gene inactivation. J Neurooncol. 2005; 73:117–24. [PubMed: 15981100]

40. Guidi CJ, Mudhasani R, Hoover K, et al. Functional interaction of the retinoblastoma and Ini1/Snf5 tumor suppressors in cell growth and pituitary tumorigenesis. Cancer Res. 2006; 66:8076–82. [PubMed: 16912184]
41. Kohashi K, Oda Y, Yamamoto H, et al. Highly aggressive behavior of malignant rhabdoid tumor: a special reference to SMARCB1/INI1 gene alterations using molecular genetic analysis including quantitative real-time PCR. J Cancer Res Clin Oncol. 2007; 133:817–24. [PubMed: 17486366]
42. Medjkane S, Novikov E, Versteege I, et al. The tumor suppressor hSNF5/INI1 modulates cell growth and actin cytoskeleton organization. Cancer Res. 2004; 64:3406–13. [PubMed: 15150092]
43. Klochendler-Yeivin A, Picarsky E, Yaniv M. Increased DNA damage sensitivity and apoptosis in cells lacking the Snf5/Ini1 subunit of the SWI/SNF chromatin remodeling complex. Mol Cell Biol. 2006; 26:2661–74. [PubMed: 16537910]
44. Jeibmann A, Buerger H, Fruhwald M, et al. No evidence for epidermal growth factor receptor amplification and overexpression in atypical teratoid/rhabdoid tumors. Acta Neuropathol. 2006; 112:513–4. [PubMed: 16896904]
45. Koos B, Jeibmann A, Lunenburger H, et al. The tyrosine kinase c-Abl promotes proliferation and is expressed in atypical teratoid and malignant rhabdoid tumors. Cancer. 2010; 116:5075–81. [PubMed: 20629032]
46. Polager S, Ginsberg D. p53 and E2f: partners in life and death. Nat Rev Cancer. 2009; 9:738–48. [PubMed: 19776743]
47. Tabori U, Baskin B, Shago M, et al. Universal poor survival in children with medulloblastoma harboring somatic TP53 mutations. J Clin Oncol. 2010; 28:1345–50. [PubMed: 20142599]
48. Pfaff E, Remke M, Sturm D, et al. TP53 mutation is frequently associated with CTNNB1 mutation or MYCN amplification and is compatible with long-term survival in medulloblastoma. J Clin Oncol. 2010; 28:5188–96. [PubMed: 21060032]
49. Eberhart CG, Chaudhry A, Daniel RW, et al. Increased p53 immunopositivity in anaplastic medulloblastoma and supratentorial PNET is not caused by JC virus. BMC Cancer. 2005; 5:19. [PubMed: 15717928]
50. Rohini K, Mathivanan J, Prabhu PD, et al. Loss of heterozygosity of the p53 gene and deregulated expression of its mRNA and protein in human brain tumors. Mol Cell Biochem. 2007; 300:101–11. [PubMed: 17180249]
51. Das P, Kotilingam D, Korchin B, et al. High prevalence of p53 exon 4 mutations in soft tissue sarcoma. Cancer. 2007; 109:2323–33. [PubMed: 17429838]
52. Salinas-Sanchez AS, Atienzar-Tobarra M, Lorenzo-Romero JG, et al. Sensitivity and specificity of p53 protein detection by immunohistochemistry in patients with urothelial bladder carcinoma. Urol Int. 2007; 79:321–7. [PubMed: 18025850]
53. Massoni Neto LM, Bianchi CP, Ab'Saber AM, et al. p53 immunostaining is correlated with reduced survival and is not correlated with gene mutations in resected pulmonary large cell carcinomas. Braz J Med Biol Res. 2007; 40:1045–53. [PubMed: 17665040]
54. Cordes C, Von Lingen J, Gorogh T, et al. Molecular and immunological aspects of p53 and p53-autoantibodies in head and neck squamous cell carcinoma. Oncol Rep. 2009; 22:1299–303. [PubMed: 19885580]
55. Xu Y, Yan W, Chen X. SNF5, a core component of the SWI/SNF complex, is necessary for p53 expression and cell survival, in part through eIF4E. Oncogene. 2010; 29:4090–100. [PubMed: 20473326]
56. Abbas T, Dutta A. p21 in cancer: intricate networks and multiple activities. Nat Rev Cancer. 2009; 9:400–14. [PubMed: 19440234]
57. Tanaka M, Sasaki H, Kino I, et al. Genes preferentially expressed in embryo stomach are predominantly expressed in gastric cancer. Cancer Res. 1992; 52:3372–7. [PubMed: 1596895]
58. Shields LB, Gercel-Taylor C, Yashar CM, et al. Induction of immune responses to ovarian tumor antigens by multiparity. J Soc Gynecol Investig. 1997; 4:298–304.
59. Nozawa Y, Van Belzen N, Van der Made AC, et al. Expression of nucleophosmin/B23 in normal and neoplastic colorectal mucosa. J Pathol. 1996; 178:48–52. [PubMed: 8778315]
60. Naoe T, Suzuki T, Kiyoi H, et al. Nucleophosmin: a versatile molecule associated with hematological malignancies. Cancer Sci. 2006; :97:963–9. [PubMed: 16984370]

61. Grisendi S, Mecucci C, Falini B, et al. Nucleophosmin and cancer. Nat Rev Cancer. 2006; 6:493–505. [PubMed: 16794633]

62. Kurki S, Peltonen K, Latonen L, et al. Nucleolar protein NPM interacts with HDM2 and protects tumor suppressor protein p53 from HDM2-mediated degradation. Cancer Cell. 2004; 5:465–75. [PubMed: 15144954]

63. Zhang H, Shi X, Paddon H, et al. B23/nucleophosmin serine 4 phosphorylation mediates mitotic functions of polo-like kinase 1. J Biol Chem. 2004; 279:35726–34. [PubMed: 15190079]

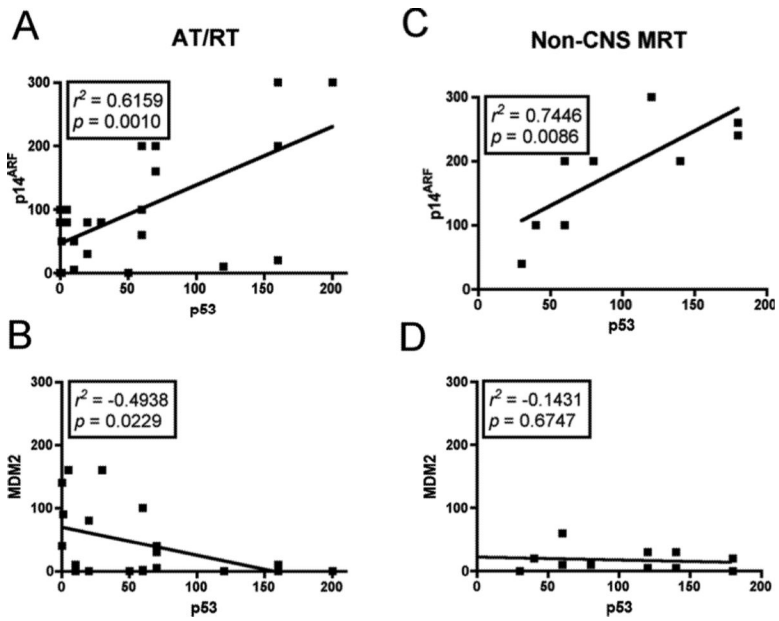

Figure 1.

Organization of tissue microarray (TMA) and scheme for staining assessment. (**A**) Hematoxylin and eosin sections of entire atypical teratoid/rhabdoid (AT/RT) and non-CNS malignant rhabdoid tumor (MRT) TMA. Shaded boxes indicate control non-tumor samples. (**B**) Illustration of the $p16^{ARF}$ and $p14^{INK4A}$ pathways. Each component of these pathways was stained on both AT/RT and non-CNS MRT TMAs. (**C**) Stained variables were scored as strong (3+), moderate (2+), weak (1+) or negative (0).

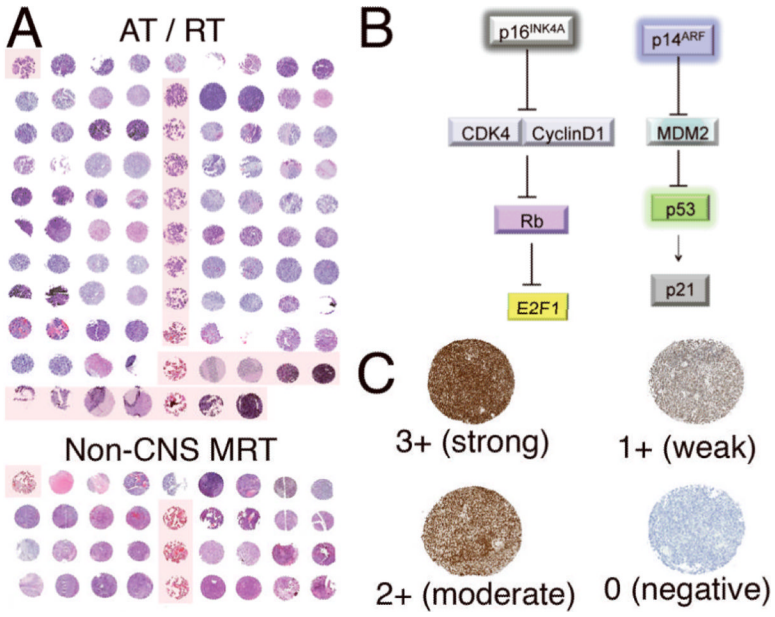

Figure 2.

Immunohistochemical expression profiles of $p21^{CIP1/WAF1}$and $p16^{INK4A}$ and $p14^{ARF}$ in atypical teratoid/rhabdoid (AT/RT) and non-CNS malignant rhabdoid tumors (MRT). (**A, B**) Representative images displaying lack of expression (score = 0) of both $p21^{CIP1/WAF1}$ (**A**) and $p16^{INK4A}$ (**B**) in AT/RT cases. (**C**) Representative image from an AT/RT case showing strong (3+) $p14^{ARF}$ expression. (**D**) Semiquantitative estimation of staining in all AT/RT and non-CNS MRT cases. $p14^{ARF}$ expression ranged from focal weak to diffuse strong staining and was higher in both AT/RT and non-CNS MRT relative to $p21^{CIP1/WAF1}$and $p16^{INK4A}$ expression. Data were analyzed using ANOVA (***$p < 0.0001$). The y-axis represents a semiquantitative measure of the product of staining intensity and percentage of positive cells in each case.

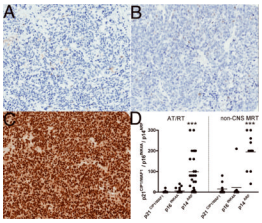

Figure 3.

Immunohistochemical expression profiles of CDK4 and cyclinD1 in atypical teratoid/rhabdoid (AT/RT) and non-CNS malignant rhabdoid tumors (MRT). (**A**) CDK4 immunostaining showed weak (1+) expression in AT/RT. (**B**) Semiquantitative estimation of CDK4 shows weak expression in both AT/RT and non-CNS MRT. (**C**) Focal weak (1+) expression of cyclin D1 staining in AT/RT. (**D**) Semiquantitative estimation of cyclinD1 showed focal weak expression in both AT/RT and non-CNS MRT. The y-axes in **B** and **D** represent a semiquantitative measure of the product of staining intensity and percentage of positive cells in each case.

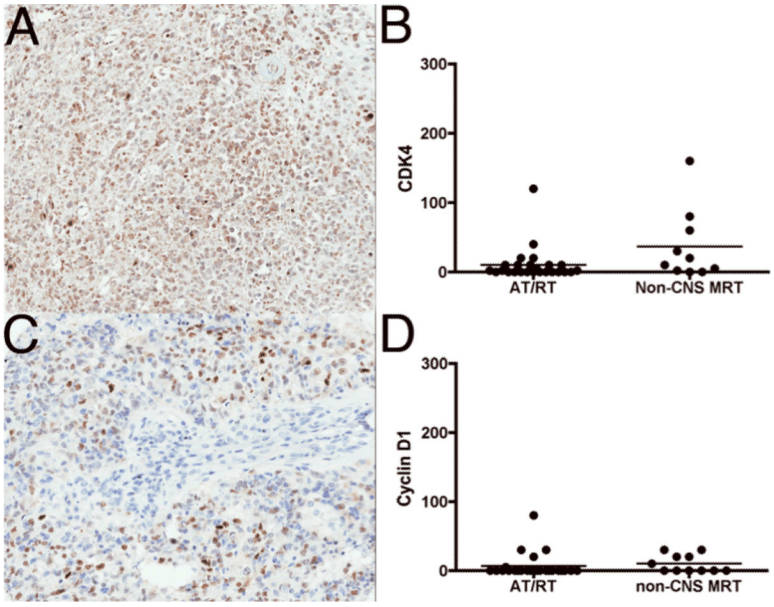

Figure 4.

Immunostaining for ppRB and E2F1 in atypical teratoid/rhabdoid (AT/RT) and non-CNS malignant rhabdoid tumor (MRT). (**A**) Moderate (2+) staining with ppRB in non-CNS MRT. (**B**) Semiquantitative estimation of ppRB staining showing focal weak to moderate expression in both AT/RT and non-CNS MRT. (**C**) Representative image demonstrating negative E2F1 staining (score = 0) in a non-CNS MRT. (**D**) Semiquantitative estimation of sE2F1 showing no staining in all cases of both AT/RT and non-CNS MRT. The y-axes in **B** and **D** represent a semiquantitative measure of the product of staining intensity and percentage of positive cells in each case.

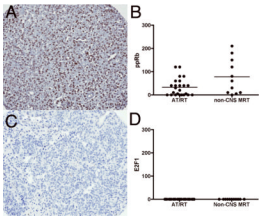

Figure 5.

Immunohistochemical expression of p53 and MDM2 in atypical teratoid/rhabdoid (AT/RT) and non-CNS malignant rhabdoid tumors (MRT). (**A**) Representative p53 immunostaining of an AT/RT case showing moderate (2+) p53 expression. (**B**) Semiquantitative estimation of p53 showed moderate to weak expression in many AT/RT and all non-CNS MRT cases. (**C**) Weak (1+) expression of MDM2 staining in an AT/RT case. (**D**) Semiquantitative estimation of MDM2 showed focal weak to moderate expression in AT/RT and non-CNS MRT cases. The y-axes in **B** and **D** represent semiquantitative measures of the product of staining intensity and percentage of positive cells in each case.

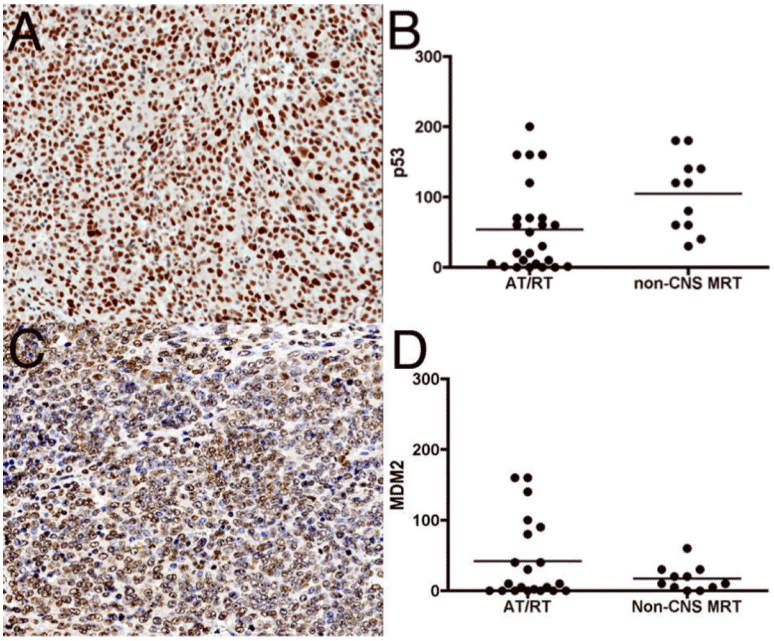

Figure 6.

Relationship between p53 and $p14^{ARF}$ / MDM2 in malignant rhabdoid tumors (MRT). Non-parametric correlations using 95% confidence intervals were performed to quantify the relationship between p53, $p14^{ARF}$ and MDM2. Results from correlation analyses are represented by r^2, the Spearman's coefficient. (**A**) Positive correlations between p53 and $p14^{ARF}$ in AT/RT. (**B**) Negative correlations between p53 and MDM2 in atypical teratoid/rhabdoid (AT/RT) tumors. (**C**) Positive correlations in non-CNS MRT between p53 and $p14^{ARF}$. (**D**) No relationship between p53 and MDM2 in non-CNS MRT.

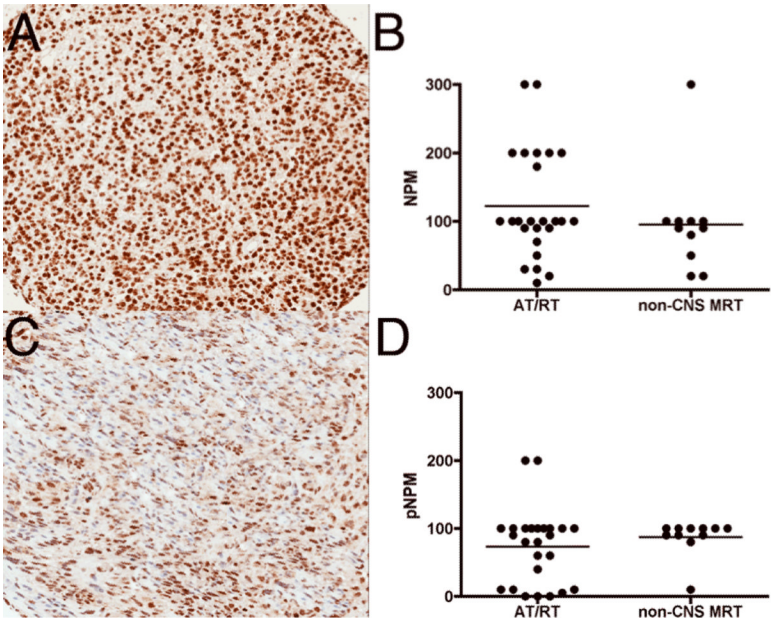

Figure 7.

Malignant rhabdoid tumors (MRT) express nucleophosmin (NPM). (**A**) NPM immunostaining of an atypical teratoid/rhabdoid (AT/RT) tumor demonstrating strong (3+) expression. (**B**) Semiquantitative estimation of NPM showed strong to weak expression in all AT/RT and non-CNS malignant rhabdoid tumor (MRT) cases. (**C**) Moderate (2+) expression of phosphorylated NPM (pNPM) in an AT/RT case. (**D**) Semiquantitative estimation of pNPM showed focal weak to moderate expression in AT/RT and non-CNS MRT cases. The y-axes in **B** and **D** represent semiquantitative measures of the product of staining intensity and percentage of positive cells in each case.

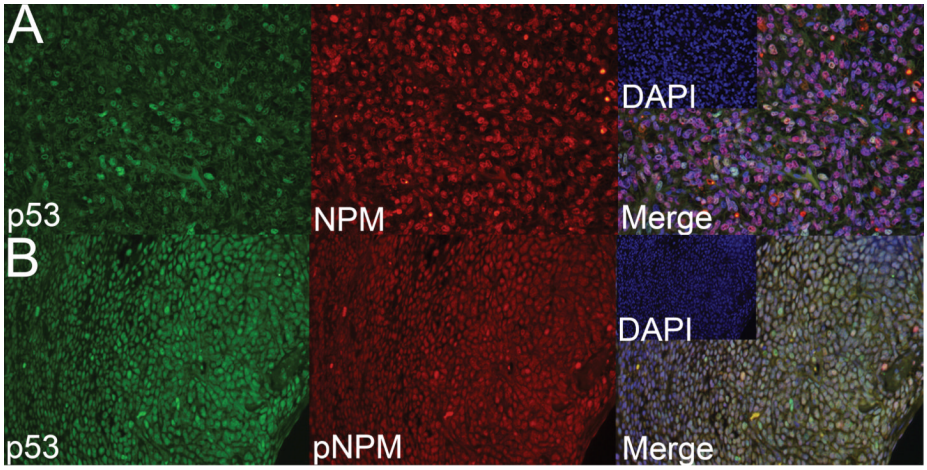

Figure 8.

Nucleophosmin (NPM) and phosphorylated NMP (pNPM) colocalize with p53 in malignant rhabdoid tumor (MRT). (**A**) Representative fluorescence immunostaining of an atypical teratoid/rhabdoid (AT/RT) case demonstrates colocalization of p53 (green) and NPM (red). Original magnification: 40×. (**B**) Representative fluorescence immunostaining on a non-CNS MRT case demonstrating colocalization of p53 (green) and pNPM (red). Original magnification: 20×. Insets shows nuclei counter stained with 4',6-diamidino-2-phenylindole (DAPI, blue).

Table 1

Patient Characteristics and *TP53* Mutational Analysis

Atypical Teratoid / Rhabdoid Tumor				
Case No.	**Age (mo)**	**Sex**	**Location**	***TP53* polymorphism/ mutation**
1	11	F	Cerebello-pontine angle	Yes
2	17	M	Brain and spinal cord	Yes
3	47	M	Cerebellum	Not assessed
4	6	M	Pineal region	Not assessed
5	9	F	Pineal region	Not assessed
6	19	M	Pineal region	Yes
7	53	M	Temporal lobe	Yes, c.722C>T (Ser>Phe)
8	21	F	Cerebellum	Yes
9	21	M	Cerebellum	Yes
10	23	F	Cervical Spinal Cord	Yes
11	96	M	Clivus	Not assessed
12	96	M	Clivus	Yes
13	19	M	Cerebellum	Yes
14	26	M	Brain, not specified	Yes
15	30	M	Brain, not specified	Yes, c.246G>A (Pro>Pro)
16	52	F	Cerebellum	Yes
17	120	M	Spine	Yes
18	9	F	Brain, not specified	Yes, c.467G>A (Arg>His), c.582T>C (Leu>Leu)
19	11	M	Cerebellum	Not assessed
20	11	M	Cerebello-pontine angle	Yes
21	44	M	Frontal lobe	Not assessed
22	44	M	Frontal lobe	Yes
23	17	M	Cerebello-pontine angle	Yes
24	13	M	4th Ventricle	Yes
25	6	F	Cerebellum	Yes

Non-CNS Malignant Rhabdoid Tumor				
Case No.	**Age mo.**	**Sex**	**Location**	***TP53* polymorphism/ mutation**
1	6	F	Neck	Yes
2	96	F	Neck	Yes
3	108	M	Cervical Lymph Node	Yes
4	52	F	Hand	Yes
5	96	M	Liver	Yes
6	240	M	Abdomen	Not assessed
7	96	M	Axilla	Not assessed
8	32	F	Liver	Yes
9	56	F	Face	Not assessed
10	40	F	Liver	Yes
11	6	F	Kidney	Yes

The tissue microarray contained 25 cases of atypical teratoird/rhabdoid tumor (AT/RT) and 11 cases of non-CNS malignant rhabdoid tumor (MRT). F = Female; M = Male; c. = codon; C = cytosine; T = thymidine; G = guanine; A = arginine= Ser = serine; Phe = phenylalanine; Pro = proline; Arg = arginine, His – histidine, Leu – Leucine.

Table 2

Antibodies and Dilutions

No.	Antibody	Host	Source	Concentration	Incubation Time
1	Cdk4	Rabbit	AbCam, Cambridge, MA	1:100	1 hour RT
2	Cyclin D1	Rabbit	AbCam	1:100	1 hour RT
3	E2F1	Mouse	AbCam	1:50	1 hour RT
4	MDM2	Mouse	AbCam	1:50	1 hour RT
5	NPM	Rabbit	Cell Signaling, Danvers, MA	1:200	Overnight 4°C
6	$p14^{ARF}$	Mouse	Cell Signaling	1:200	Overnight 4°C
7	$p16^{INK4A}$	Mouse	MTM laboratories, Westborough, MA	Prediluted	1 hour RT
8	p21	Rabbit	Cell Signaling	1:200	Overnight 4°C
9	p53	Mouse	Dako, Carpinteria, CA	1:50	1 hour RT
10	pNPM	Rabbit	Cell Signaling	1:100	Overnight 4°C
11	ppRB	Rabbit	Cell Signaling	1:50	Overnight 4°C

CDK4 = Cyclin dependent kinase; NPM = Nucleophosmin; pNPM = phosphorylated nucleophosmin; ppRB = hyperphosphorylated form of pRb.

J Neuropathol Exp Neurol. Author manuscript; available in PMC 2012 July 1.

Table 3

Summary of Data

Atypical Teratoid/Rhabdoid Tumors (n = 25)					
		Positive			Negative
Name	Total positive	1	2	3	0
$p16^{INK4A}$	8 (32%)	8 (32%)	0 (0%)	0 (0%)	17 (68%)
CDK4	13 (52%)	12 (48%)	1 (4%)	0 (0%)	12 (48%)
Cyclin D1	5 (20%)	5 (20%)	0 (0%)	0 (0%)	20 (80%)
pRB	16 (64%)	14 (56%)	2 (8%)	0 (0%)	9 (36%)
E2F1	0 (0%)	0 (0%)	0 (0%)	0 (0%)	25 (100%)

Non CNS Malignant Rhabdoid Tumors (n = 11)					
		Positive			Negative
Name	Total positive	1	2	3	0
$p16^{INK4A}$	7 (64%)	6 (56%)	0 (0%)	1 (9%)	4 (36%)
CDK4	8 (73%)	7 (64%)	1 (9%)	0 (0%)	3 (27%)
Cyclin D1	5 (45%)	5 (45%)	0 (0%)	0 (0%)	6 (55%)
pRB	10 (91%)	6 (56%)	3 (27%)	1 (9%)	1 (9%)
E2F1	0 (0%)	0 (0%)	0 (0%)	0 (0%)	11 (100%)

Atypical Teratoid/Rhabdoid Tumors (n = 25)					
		Positive			Negative
Name	Total positive	1	2	3	0
$p14^{ARF}$	21 (84%)	6 (24%)	13 (52%)	2 (8%)	4 (16%)
MDM2	18 (72%)	14 (56%)	4 (16%)	0 (0%)	7 (28%)
p53	21 (84%)	16 (64%)	5 (20%)	0 (0%)	4 (16%)
$p21^{CIP1/WAF1}$	3 (12%)	3 (12%)	0 (0%)	0 (0%)	22 (88%)
NPM	25 (100%)	17 (68%)	6 (24%)	2 (8%)	0 (0%)
pNPM	22 (88%)	20 (80%)	2 (8%)	0 (0%)	3 (12%)

Non CNS Malignant Rhabdoid Tumors (n = 11)					
		Positive			Negative
Name	Total positive	1	2	3	0
$p14^{ARF}$	11 (100%)	3 (27%)	6 (55%)	2 (18%)	0 (0%)
MDM2	9 (82%)	9 (82%)	0 (0%)	0 (0%)	2 (18%)
p53	11 (100%)	5 (46%)	4 (36%)	2 (18%)	0 (0%)
$p21^{CIP1/WAF1}$	5 (45%)	5 (45%)	0 (0%)	0 (0%)	6 (55%)
NPM	11 (100%)	10 (91%)	0 (0%)	1 (9%)	0 (0%)
pNPM	11 (100%)	11 (100%)	0 (0%)	0 (0%)	0 (0%)

ARF = Alternative Reading Frame; CDK4 = Cyclin dependent kinase 4; CIP1 = Cyclin dependent kinase inhibitory protein 1; INK4a = Inhibitor of Kinase 4; NPM = Nucleophosmin; pNPM = phophorylated nucleophosmin; WAF1 = Wild-type activating fragment-1.